Single-shot deflectometry using an inverse crossed fringe pattern

Christian Kludt[1] and Jürgen Beyerer[12]

[1] Fraunhofer Institute of Optronics,
System Technologies and
Image Exploitation (IOSB),
Fraunhoferstr. 1, 76131 Karlsruhe
[2] Karlsruhe Institute of Technology,
Kaiserstr. 12, 76131 Karlsruhe

Abstract Phase Measuring Deflectometry (PMD) enables highly sensitive defect detection on specular surfaces but is limited by fringe pattern compression on strongly curved geometries and by the need for multiple phase-shifted exposures. We address both challenges by combining inverse fringe patterns and Fourier-domain single-shot phase retrieval. Using experimentally determined camera-screen correspondences, inverse fringe patterns are computed such that their reflections appear undistorted and spatially periodic in the camera image, without requiring explicit system calibration. Based on these predistorted patterns, a single crossed-fringe image is evaluated using Fourier-domain phase retrieval with single-sideband demodulation (SSD), enabling robust phase extraction from a single exposure. The proposed method eliminates phase shifting, reduces acquisition time, improves robustness against motion and vibration, and extends deflectometry to complex surface geometries and dynamic inspection scenarios.

Keywords Single-shot deflectometry, inverse fringe pattern, Fourier-domain phase retrieval, computational imaging, specular surface inspection, high-speed optical inspection, surface gradient measurement

1 Introduction

PMD is a widely used optical measurement technique for specular surface inspection. In conventional PMD, the two orthogonal gradient components are obtained by displaying and capturing sequences of phase-shifted sinusoidal fringe patterns. Although this approach provides high measurement accuracy, it suffers from two fundamental limitations.

First, surfaces with steep slopes and strong curvatures lead to severe distortion and spatial compression of the reflected fringe patterns in the camera image. The observed fringes become locally dense and irregular. If the fringe frequency exceeds the spatial resolution of the imaging sensor, reliable phase extraction is no longer possible. This limitation restricts the applicability of conventional PMD for objects with complex geometries that are frequently encountered in industrial inspection.

Second, phase retrieval in PMD typically relies on phase-shifting techniques requiring multiple sequential exposures. As a result, the measurement process is inherently time-consuming and sensitive to object motion, vibrations, and environmental disturbances. These limitations make conventional PMD unsuitable for high-speed measurements and dynamic inspection scenarios.

In this work, we propose a single-shot deflectometry method based on inverse fringe patterns. The key idea is to predistort the displayed fringe pattern such that, after reflection at the nominal object geometry, the fringe pattern observed by the camera becomes straight and spatially periodic. In contrast to conventional PMD, geometric distortions caused by the nominal object shape are compensated before image acquisition.

This has two important consequences. First, fringe compression is avoided, resulting in improved spatial sampling across the entire field of view. Second, the observed fringe pattern closely resembles an ideal carrier signal, providing optimal conditions for Fourier-domain phase retrieval. Consequently, phase information can be extracted from a single camera frame using Fourier-domain phase retrieval and SSD.

2 Related Work

Conventional phase-measuring deflectometry relies on phase-shifting techniques requiring multiple exposures for phase retrieval. To overcome this limitation, several single-shot approaches have been proposed. A fundamental contribution is the Fourier-transform method introduced by Takeda et al. [1], which enables phase retrieval from a single fringe image by isolating a carrier component in the frequency domain. Combined with SSD, the method allows efficient extraction of phase information without phase shifting. Liu et al. [2] demonstrated its applicability to deflectometry using crossed fringe patterns.

A common challenge of Fourier-based methods is their dependence on a well-defined carrier frequency and sufficient spectral separation. Surface-induced distortions alter the local fringe frequency and orientation, causing spectral broadening and overlap of the sidebands with the zero-order component. As a consequence, phase retrieval becomes increasingly unreliable for strongly curved or freeform specular surfaces. To address this problem, several single-shot deflectometry methods have been developed that operate directly on crossed fringe patterns. Li et al. [3] combined crossed fringes with Fourier-domain demodulation after background and modulation normalization. Nguyen et al. [4] proposed a one-shot method based on first- and second-order derivatives of the fringe image under the assumption of slowly varying background illumination and modulation. For defect detection applications, Pösch et al. [5] analyzed local fringe orientations using a short-time discrete Fourier transform and subsequent skeletonization. While these approaches eliminate phase shifting, their performance remains affected by geometric fringe distortions caused by the object shape.

A complementary line of research aims at compensating such distortions through pattern adaptation. If information about the nominal object geometry is available, the displayed pattern can be modified such that a desired fringe structure is observed in the camera image. Massig et al. [6] used predistorted crossed fringes to compensate the reflection geometry of the human eye, resulting in approximately regular fringes in the captured image. However, their approach was demonstrated only for simple near-spherical geometries. For more general objects, Li et al. [7] generated inverse fringe patterns from experimentally determined camera-screen correspondences obtained by phase-

measuring deflectometry. Werling and Beyerer [8] followed a similar inversion strategy for specular surface inspection, while Strohmeier et al. [9] demonstrated Fourier-based evaluation of inverse patterns for solely one-dimensional fringe structures.

The method proposed in this paper builds upon these two research directions. Similar to previous work on inverse fringe patterns, the displayed pattern is adapted to the nominal object geometry using experimentally determined camera-screen correspondences. In contrast to existing approaches, the resulting reflected fringe image is specifically designed to satisfy the requirements of Fourier-domain phase retrieval of crossed fringes. The inverse pattern compensates geometry-induced fringe distortion before image acquisition, thereby preventing fringe compression and improving spectral separation in the Fourier domain. This enables robust single-shot phase retrieval using SSD even for strongly curved and freeform specular surfaces.

The main contributions of this work are:

- A fast and robust algorithm for generating inverse fringe patterns from experimentally determined camera-screen correspondences.
- A calibration-free black-box implementation that does not require explicit knowledge of intrinsic or extrinsic system parameters.
- A single-shot deflectometry method based on inverse crossed fringe patterns and Fourier-domain phase retrieval.

3 Proposed Method

When a pattern displayed on a screen is observed via a specular surface, its appearance in the camera image is generally distorted by the object's geometry. This effect can be exploited in reverse. Assuming that a deflectometric reference measurement of the test object is available, inverse fringe patterns can be generated such that, after reflection at the object surface, a predefined fringe pattern appears in the camera image. The displayed pattern therefore contains a compensating geometric distortion which cancels the distortion introduced by the object's shape.

For this purpose we use the phase shifting method [10]. It is extensively used in deflectometry [11] for its robustness against the transmission impairments attenuation, blurring and noise. In the following, we introduce the subscripts $_\mathrm{c}$ and $_\mathrm{s}$ to indicate camera and screen quantities, respectively. To this end, each screen pixel position $\mathbf{x}_\mathrm{s}$ is encoded via a temporal sequence of discrete gray values, the so-called phase shifting sequence. Recording and decoding it yields the deflectometric registration $\boldsymbol{\xi}$, a function

$$\boldsymbol{\xi} : \mathcal{C} \mapsto \mathcal{S} \cup \varnothing, \quad \mathcal{C} \subseteq \mathbb{Z}^2, \quad \mathcal{S} \subseteq \mathbb{R}^2 \tag{1}$$

from the two-dimensional set of all camera pixels $\mathcal{C}$ to the two-dimensional set of screen positions $\mathcal{S}$ (with the empty set representing no interception), yielding estimated screen positions $\hat{\mathbf{x}}_\mathrm{s}$ for every camera pixel $\mathbf{x}_\mathrm{c}$:

$$\boldsymbol{\xi}(\mathbf{x}_\mathrm{c}) = \hat{\mathbf{x}}_\mathrm{s}, \quad \text{with} \quad \mathbf{x}_\mathrm{c} = \begin{pmatrix} x_\mathrm{c} \\ y_\mathrm{c} \end{pmatrix}, \quad \hat{\mathbf{x}}_\mathrm{s} = \begin{pmatrix} \hat{x}_\mathrm{s} \\ \hat{y}_\mathrm{s} \end{pmatrix}. \tag{2}$$

In the same way an image I_α can be modeled as a function

$$I_\alpha : \Omega_\alpha \mapsto \mathcal{I}, \quad \mathcal{I} \subseteq \mathbb{R} \tag{3}$$

from the support points Ω_α to image values $\mathcal{I}$, assigning an image value i_α to every position $\mathbf{x}$, with $\alpha \in \{\mathrm{c}, \mathrm{s}\}$:

$$I_\alpha(\mathbf{x}) = i_\alpha. \tag{4}$$

During a deflectometric measurement an image I_s is displayed on the screen, reflected by the test object and captured with a camera as the image I_c. Then $\boldsymbol{\xi}$ is the geometric transformation of the scene which maps I_s to I_c:

$$I_\mathrm{c}(\mathbf{x}_\mathrm{c}) = I_\mathrm{s}(\boldsymbol{\xi}(\mathbf{x}_\mathrm{c})). \tag{5}$$

In order to generate an image I'_s which compensates $\boldsymbol{\xi}$, we need its inverse function $\boldsymbol{\xi}^{-1} : \mathcal{S} \mapsto \mathcal{C}$. However, this presents an ill-posed problem for the following reasons:

- $\boldsymbol{\xi}^{-1}$ is not well defined because there may be screen positions $\mathbf{x}_\mathrm{s}$ where no camera sight ray is looking at, so that $\boldsymbol{\xi}$ is not surjective.
- $\boldsymbol{\xi}^{-1}$ is not uniquely defined because there might be more than one camera sight ray looking at the same screen positions $\hat{\mathbf{x}}_\mathrm{s}$, so that $\boldsymbol{\xi}$ is not injective. In fact, the inverse is a multivalued function $\boldsymbol{\xi}^{-1} : \mathcal{S} \rightrightarrows \mathcal{C} \cup \varnothing$.
- $\boldsymbol{\xi}^{-1}$ is not continuous: although screen positions $\hat{\mathbf{x}}_\mathrm{s}$ are decoded with continuous values, the two-dimensional set of discrete screen pixels $\tilde{\mathcal{S}}$ can only be activated at discrete pixels $\mathbf{x}_\mathrm{s} \in \tilde{\mathcal{S}} \subseteq \mathbb{Z}^2$.

Because the registration $\boldsymbol{\xi}$ is neither surjective nor injective, it follows that it is not bijective, hence it is not invertible.

As a regularization constraint, we assume a certain degree of smoothness. While this assumption may be violated for objects containing steep slopes or discontinuities, the inverse mapping $\boldsymbol{\xi}^{-1}$ is assumed to be piecewise continuous within local neighborhoods. As a local support region we use a circular neighborhood with radius r chosen according to the projected circle of confusion of a camera sight ray on the screen. With this, we assign an interpolated gray value i'_s to each screen pixel $\mathbf{x}_\mathrm{s}$ as follows:

First, the Euclidean distance between an integer screen pixel position $\mathbf{x}_\mathrm{s}$ and a decoded screen position $\hat{\mathbf{x}}_\mathrm{s} = \boldsymbol{\xi}(\mathbf{x}_\mathrm{c})$ is denoted by

$$d(\mathbf{x}_\mathrm{s}, \hat{\mathbf{x}}_\mathrm{s}) = \|\mathbf{x}_\mathrm{s} - \hat{\mathbf{x}}_\mathrm{s}\|. \tag{6}$$

Second, the set of all camera pixels $\mathbf{x}_\mathrm{c}$ where d evaluates to zero is denoted by

$$\mathcal{C}^0(\mathbf{x}_\mathrm{s}) = \{\mathbf{x}_\mathrm{c} \in \mathcal{C} \mid d(\mathbf{x}_\mathrm{s}, \hat{\mathbf{x}}_\mathrm{s}) = 0\}. \tag{7}$$

Third, the set of all camera pixels $\mathbf{x}_\mathrm{c}$ where d is within the radius r is denoted by

$$\mathcal{C}^r(\mathbf{x}_\mathrm{s}) = \{\mathbf{x}_\mathrm{c} \in \mathcal{C} \mid 0 < d(\mathbf{x}_\mathrm{s}, \hat{\mathbf{x}}_\mathrm{s}) \leq r\}. \tag{8}$$

Fourth, we apply inverse distance weighting [12] using the modified [13] Shepard's method with the weights

$$w(\mathbf{x}_\mathrm{c}) = \begin{cases} d(\mathbf{x}_\mathrm{s}, \hat{\mathbf{x}}_\mathrm{s})^{-2}, & \text{if} \quad d \leq r, \\ 0, & \text{otherwise.} \end{cases} \tag{9}$$

Given an image I_c with image values i_c which we want to capture with the camera, we compute the pixel values i'_s of the converted image by setting the value of the screen pixel $\mathbf{x}_\mathrm{s}$ to the mean value of all image values i_c where the distance d evaluates to zero; the inverse distance weighted mean of the pixel values where the distance is larger than zero but smaller than or equal to the radius r; and zero if no distance value is within the radius r:

$$i'_\mathrm{s} = \begin{cases} \frac{\sum_{\mathbf{x}_\mathrm{c} \in \mathcal{C}^0} I_\mathrm{c}(\mathbf{x}_\mathrm{c})}{|\mathcal{C}^0|}, & \text{if} \quad |\mathcal{C}^0| > 0 \\ \frac{\sum_{\mathbf{x}_\mathrm{c} \in \mathcal{C}^r} w(\mathbf{x}_\mathrm{c}) I_\mathrm{c}(\mathbf{x}_\mathrm{c})}{\sum_{\mathbf{x}_\mathrm{c} \in \mathcal{C}^r} w(\mathbf{x}_\mathrm{c})} & \text{if} \quad |\mathcal{C}^r| > 0 \\ 0, & \text{otherwise.} \end{cases} \tag{10}$$

When using a *kd-tree* as a fast spatial search structure, this becomes an efficient interpolation method with computational complexity $\mathcal{O}(|\tilde{\mathcal{S}}| \log(|\mathcal{C}|))$ for queries.

A significant advantage of this procedure is that it does not require explicit calibration of either camera or screen. The complete system is treated as a black box, and all required information is obtained experimentally. As a result, system setup is simplified and automated deployment becomes possible.

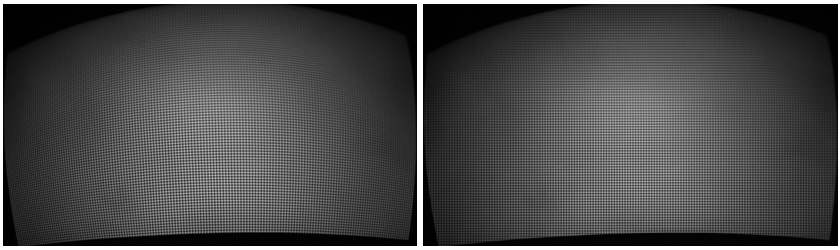
4 Experimental Setup

The experimental setup consists of a flat-panel display for fringe pattern projection, a monochrome camera for image acquisition, and a workstation for inverse fringe pattern generation and phase evaluation. A convex mirror was used as a representative specular test object exhibiting pronounced curvature and strong geometric distortion of reflected fringe patterns.

First, a conventional phase-measuring deflectometric reference measurement was performed to determine the camera-screen correspondence ξ. The acquired registration was subsequently used to generate inverse fringe patterns according to the method described in Section 3. No explicit geometric calibration of the camera, screen, or object was required, as the inversion procedure operates directly on the experimentally determined correspondence data.

During measurement, the inverse crossed fringe pattern was displayed on the screen and observed through reflection at the specular test object, cf. Fig. 1. The carrier frequencies of the conventional and inverse fringe patterns were chosen such that both reflected patterns exhibit identical spatial frequencies in the camera image.

Finally, the recorded images were processed using Fourier-based SSD to recover the phase information.

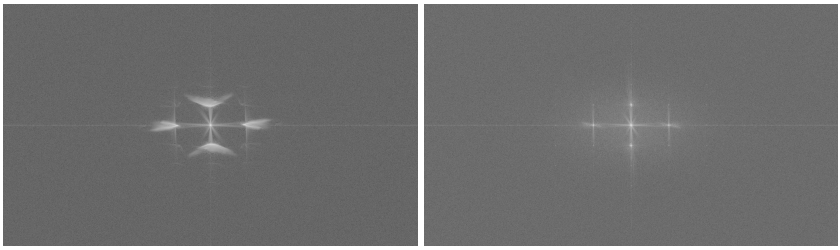


(a) distorted **(b)** inverse

Figure 1: Crossed fringe patterns, both with a spatial frequency $\nu \approx (12 pixel)^{-1}$. The inverse pattern appears undistorted and geometrically regular after reflection.

5 Results and Discussion

The generated inverse fringe patterns successfully compensate the dominant geometric distortions introduced by the nominal object shape. Figure 1 shows that the reflected inverse fringe pattern remains straight and spatially uniform over the entire field of view. In contrast, the conventional fringe pattern exhibits pronounced local compression and distortion caused by the surface curvature of the test object.



(a) distorted **(b)** inverse

Figure 2: Fourier spectra (absolute values, logarithmic scale) of the crossed fringe patterns. The spectrum of the inverted pattern exhibits stronger and more distinct peaks.

The improved spatial regularity is directly reflected in the Fourier domain. Figure 2 compares the spectra of conventionally acquired and inverse fringe patterns. For the conventional measurement, geometric fringe distortions broaden the sidebands and reduce their separation from the low-frequency and DC-components. In contrast, the inverse fringe pattern produces well localized spectral peaks and a significantly narrower spectral distribution.

These spectral properties are particularly advantageous for SSD. The improved separation of the carrier frequencies enables more selective frequency-domain filtering and reduces leakage from neighboring spectral components. Consequently, phase retrieval becomes more robust and less sensitive to geometric distortions of the object under investigation.

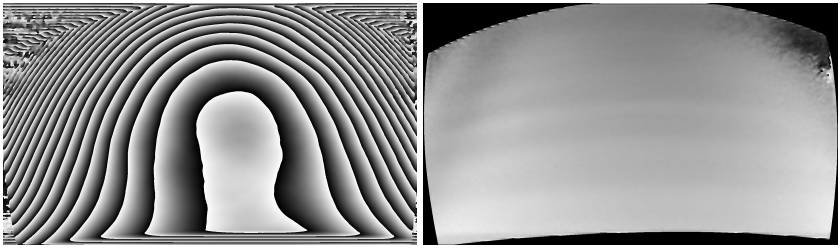
The displayed crossed fringe pattern is characterized by its spatial carrier frequency. After reflection at the specular test object, this carrier is locally modulated by the object's shape and surface slopes, resulting in spatially varying fringe frequencies and distortions.

In contrast, the proposed inverse fringe pattern is pre-distorted such that the modulation introduced by the nominal object geometry is compensated during reflection. Consequently, the fringe pattern observed by the camera exhibits an approximately constant carrier frequency across the field of view.

Figure 3 shows the phase maps recovered from a single camera exposure. After shifting the selected sideband to the frequency origin

for SSD, the phase recovered from the conventional fringe pattern contains the expected phase wraps corresponding to the object-induced modulation, whereas the inverse fringe pattern yields a largely flattened phase distribution because the dominant form contribution has already been compensated during pattern generation.

The results demonstrate that compensating geometric fringe distortions before acquisition establishes favorable conditions for Fourier-domain phase retrieval and enables reliable single-shot deflectometric evaluation.



(a) distorted **(b)** inverse

Figure 3: Fourier-domain phase retrieval with single-sideband demodulation (SSD). The values range from 0 (black) to 2π (white).

6 Conclusion

This paper presented a single-shot deflectometry method that combines inverse crossed fringe patterns with Fourier-domain phase retrieval. Using experimentally determined camera-screen correspondences, inverse crossed fringe patterns are generated such that their reflections appear spatially periodic and geometrically regular in the camera image, without requiring explicit geometric calibration of the measurement system.

The experimental results demonstrate that compensating the nominal object geometry prior to image acquisition substantially reduces fringe compression on strongly curved specular surfaces and improves the spectral separation of the carrier frequencies. As a consequence, the acquired fringe images provide favorable conditions for SSD, enabling

robust phase retrieval from a single exposure. The proposed method therefore combines the geometric advantages of inverse fringe compensation with the speed and simplicity of Fourier-based single-shot evaluation.

References

1. M. Takeda, H. Ina, and S. Kobayashi, "Fourier-transform method of fringe-pattern analysis for computer-based topography and interferometry," *Journal of the Optical Society of America*, vol. 72, no. 1, p. 156, Jan. 1982. [Online]. Available: https://opg.optica.org/abstract.cfm?URI=josa-72-1-156
2. Y. Liu, E. Olesch, Z. Yang, and G. Häusler, "Fast and accurate deflectometry with crossed fringes," *Advanced Optical Technologies*, vol. 3, no. 4, pp. 441–445, Aug. 2014. [Online]. Available: https://www.frontiersin.org/articles/10.1515/aot-2014-0032
3. W. Li, T. Bothe, M. K. Kalms, C. Von Kopylow, and W. P. O. Jueptner, "Applications of inverse pattern projection," W. Osten, M. Kujawinska, and K. Creath, Eds., Munich, Germany, May 2003, p. 492. [Online]. Available: http://proceedings.spiedigitallibrary.org/proceeding.aspx?doi=10.1117/12.508367
4. M. T. Nguyen, Y.-S. Ghim, and H.-G. Rhee, "One-shot deflectometry for high-speed inline inspection of specular quasi-plane surfaces," *Optics and Lasers in Engineering*, vol. 147, p. 106728, Dec. 2021. [Online]. Available: https://linkinghub.elsevier.com/retrieve/pii/S0143816621001986
5. A. Pösch, T. Vynnyk, and E. Reithmeier, "Using inverse fringe projection to speed up the detection of local and global geometry defects on free-form surfaces," P. J. Bones, M. A. Fiddy, and R. P. Millane, Eds., San Diego, California, USA, Oct. 2012, p. 85000B. [Online]. Available: http://proceedings.spiedigitallibrary.org/proceeding.aspx?doi=10.1117/12.928700
6. J. H. Massig, E. Lingelbach, and B. Lingelbach, "Videokeratoscope for accurate and detailed measurement of the cornea surface," *Applied Optics*, vol. 44, no. 12, p. 2281, Apr. 2005. [Online]. Available: https://opg.optica.org/abstract.cfm?URI=ao-44-12-2281
7. W. Li, T. Bothe, W. Osten, and M. Kalms, "Object adapted pattern projection—Part I: generation of inverse patterns," *Optics and Lasers in Engineering*, vol. 41, no. 1, pp. 31–50, Jan. 2004. [Online]. Available: https://linkinghub.elsevier.com/retrieve/pii/S0143816602001161

8. S. Werling and J. Beyerer, "Automatische Inspektion spiegelnder Oberflächen mittels inverser Muster (Inspection of Specular Surfaces with Inverse Patterns)," *tm - Technisches Messen*, vol. 74, no. 4, pp. 217–223, Apr. 2007. [Online]. Available: https://www.degruyterbrill.com/document/doi/10.1524/teme.2007.74.4.217/html
9. M. Strohmeier, M. Schröder, and C. Faber, "Optical inline inspection detecting 3D defects on complex free-form surfaces in harsh production environments," *tm - Technisches Messen*, vol. 86, no. 6, pp. 335–344, May 2019. [Online]. Available: https://www.degruyter.com/document/doi/10.1515/teme-2019-0013/html
10. M. Servin, J. A. Quiroga, and J. M. Padilla, Eds., *Fringe Pattern Analysis for Optical Metrology: Theory, Algorithms, and Applications*, 1st ed. Wiley, Jul. 2014. [Online]. Available: https://onlinelibrary.wiley.com/doi/book/10.1002/9783527681075
11. J. Burke, A. Pak, S. Höfer, M. Ziebarth, M. Roschani, and J. Beyerer, "Deflectometry for specular surfaces: an overview," *Advanced Optical Technologies*, vol. 12, p. 1237687, Jul. 2023. [Online]. Available: https://www.frontiersin.org/articles/10.3389/aot.2023.1237687
12. D. Shepard, "A two-dimensional interpolation function for irregularly-spaced data," in *Proceedings of the 1968 23rd ACM national conference on -*. Not Known: ACM Press, 1968, pp. 517–524. [Online]. Available: http://portal.acm.org/citation.cfm?doid=800186.810616
13. R. J. Renka, "Multivariate interpolation of large sets of scattered data," *ACM Transactions on Mathematical Software*, vol. 14, no. 2, pp. 139–148, Jun. 1988. [Online]. Available: https://dl.acm.org/doi/10.1145/45054.45055